


RESEARCH ARTICLE

Feedback field control improves the precision of T_2^* quantification at 7 T

Michael Wyss¹  | Yolanda Duerst¹ | Daniel Nanz² | Lars Kasper^{1,3} | Bertram Jakob Wilm¹ | Benjamin Emmanuel Dietrich¹ | Simon Gross¹ | Thomas Schmid¹ | David Otto Brunner¹ | Klaas Paul Pruessmann¹

¹University of Zurich and ETH Zurich Institute for Biomedical Engineering, Zurich, Switzerland

²University Hospital Zurich Institute of Diagnostic and Interventional Radiology, Zurich, Switzerland

³University of Zurich and ETH Zurich Translational Neuromodeling Unit, Zurich, Switzerland

Correspondence

K. P. Pruessmann, University of Zurich and ETH Zurich Institute for Biomedical Engineering, Zurich, Switzerland.
Email: pruessmann@biomed.ee.ethz.ch

Funding information

Swiss Commission for Technology and Innovation

T_2^* mapping offers access to a number of important structural and physiological tissue parameters. It is robust against RF field variations and overall signal scaling. However, T_2^* measurement is highly sensitive to magnetic field errors, including perturbations caused by breathing motion at high baseline field. The goal of this work is to assess this issue in T_2^* mapping of the brain and to study the benefit of field stabilization by feedback field control.

T_2^* quantification in the brain was investigated by phantom and *in vivo* measurements at 7 T. Repeated measurements were made with and without feedback field control using NMR field sensing and dynamic third-order shim actuation. The precision and reliability of T_2^* quantification was assessed by studying variation across repeated measurements as well as fitting errors. Breathing effects were found to introduce significant error in T_2^* mapping results. Field control mitigates this problem substantially. In a phantom it virtually eliminates the effects of emulated breathing fluctuations in the head. *In vivo* it enhances the structural fidelity of T_2^* maps and reduces fitting residuals along with standard deviation.

In conclusion, feedback field control improves the fidelity of T_2^* mapping in the presence of field perturbations. It is an effective means of countering bulk susceptibility effects of breathing and hence holds particular promise for efforts to leverage high field for T_2^* studies *in vivo*.

KEYWORDS

7 tesla, field control, magnetic field monitoring, NMR field probes, shim feedback, T_2^* -quantification

1 | INTRODUCTION

Gradient echo sequences with long echo times are particularly useful in high-field brain imaging due to high tissue contrast and moderate specific absorption rate (SAR).^{1,2} The resulting images can however be compromised by inhomogeneity of the transmit field (B_1^+) and varying receive-coil sensitivity profiles. In contrast, quantitative T_2^* mapping is not affected by such variations or by overall signal scaling and other imaging parameters. This is an advantage in the domain of ultra-high-field imaging, especially in the absence of a multi-channel transmit system. Quantitative T_2^* values potentially hold information on several physiological tissue parameters. For example, they sensitively respond to tissue-iron variations and are, thus, valuable in brain-iron studies.¹ It has been shown that both the chemical state and the concentration of brain-tissue iron vary with age and are altered in neurodegenerative disorders, such as Parkinson's and Alzheimer's disease, multiple sclerosis and other iron-related central nervous system (CNS) disorders.^{1,3-5} T_2^* decay times have also been shown to inversely correlate with myelin content⁶ and to depend on the organization and orientation of the myelin architecture. Thus, ultra-high-field MR scanners open possibilities to study cortical myelo-architecture patterns *in vivo* by T_2^* mapping.⁷

However, all gradient echo based sequences and methods based on long echo times such as transverse relaxation-weighted imaging (T_2^*), T_2^* mapping, susceptibility-weighted imaging (SWI) or quantitative susceptibility mapping (QSM) are very sensitive to magnetic field variations and require a spatially homogeneous and temporally stable magnetic field. Spatiotemporal magnetic field fluctuations lead to a degraded image quality

in MRI. Severe image artifacts such as ghosting, blurring or signal loss in brain imaging have been reported.^{8,9} However, in a patient examination the field is known to fluctuate for various reasons, such as hardware imperfections or patient-related effects such as breathing or limb motion.^{8,10-13} The amplitudes of patient-related fluctuations scale with the main static magnetic field strength and become particularly prominent at field strengths above 3 T.⁹ The intention of T_2^* mapping as a quantitative measurement is to deliver precise, robust and reliable results. The derivation of T_2^* values is expected to benefit from field stabilization in particular, as it involves T_2^* -weighted sequences that acquire multiple echo times without intermittent refocusing RF pulses. It is anticipated that the data quality and consistency of the late echoes, in particular, will improve, and thereby a correspondingly improved fitting precision is expected.

To compensate for spatiotemporal field perturbations, retrospective data correction based on phase navigators^{8,14,15} or magnetic field monitoring¹⁶⁻¹⁸ have been proposed. Another possibility is to correct for spatiotemporal field changes during the MR acquisition in real time, using a field control system based on NMR field probes.¹⁹ Real-time field control was shown to efficiently remove respiration-induced spatiotemporal field changes and stabilize the magnetic field.^{19,20} It was also shown to substantially reduce image artifacts (ghosting, blurring and signal loss) in T_2^* -weighted brain imaging at a field strength of 7 T.²¹

In this work we explore the effect of field perturbations on T_2^* quantification in the brain and investigate the benefit of field stabilization using a real-time feedback field control system.

2 | METHODS

2.1 | Study design

All experiments were performed on a 7 T MRI system (Achieva, Philips Healthcare, Cleveland, OH, USA) using a 32-channel receive coil (Nova Medical, Wilmington, DE, USA). The utility of the field control system in the context of T_2^* mapping was explored with phantom experiments and *in vivo* with a total of six volunteers. To assess the reliability and precision of T_2^* quantification, repeated measurements were made with constant sequence parameters.

2.2 | Feedback field control system

For field stabilization a real-time field control system as described by Duerst et al.¹⁹ was used. It is a standalone system and operates independently from the image acquisition. The spatiotemporal field evolution during the scan was measured using 16 fluorine-based NMR field probes^{22,23} arranged cylindrically around the 32-channel receive coil. The field-probe excitation and readout was triggered by the imaging sequence every 50 ms. The field-probe signal was acquired for 2 ms (*in vivo*) or 10 ms (phantom) and processed on a separate stand-alone spectrometer described by Dietrich et al.²⁴ A proportional-integral controller was used to calculate the corrections needed after each measurement. The correction was applied via a third-order spherical harmonics shim system (Resonance Research, Billerica, MA, USA) independently from the image acquisition. The closed loop bandwidth of the field control system was about 2 Hz, which was found to be sufficient to correct for respiration-induced field changes.²¹

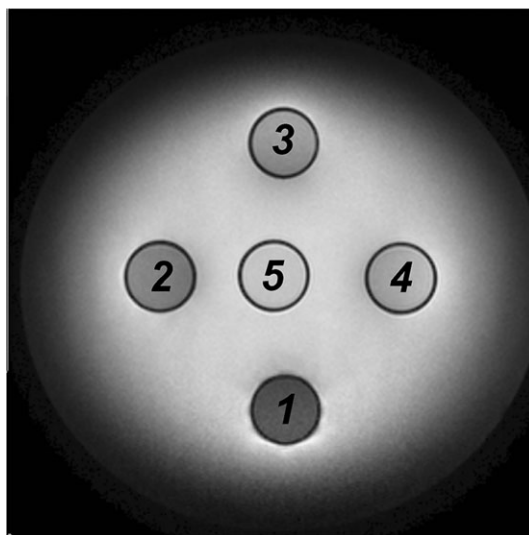


FIGURE 1 Phantom with five plastic vials placed in a container bottle. The container bottle and the vials, filled with purified water, were doped with various amounts of copper sulfate to achieve a range of T_2 values comparable to *in vivo* situations. (1, 10 ms; 2, 20 ms; 3, 30 ms; 4, 40 ms; 5, 50 ms)

2.3 | Phantom experiments

For the *in vitro* experiments, a phantom with five plastic vials (8 mL) was placed in a round supporter container with a diameter of 12 cm (Figure 1). The supporter container and the vials were filled with purified water doped with copper sulfate pentahydrate ($\text{CuSO}_4 \cdot 5\text{H}_2\text{O}$) to achieve a range of representative T_2 relaxation times. T_2 relaxation times ranged from 10 to 50 ms for the liquids within the vials and 80 ms for the fluid in the container. The concentrations (g CuSO_4 /L) of the liquids for the T_2 relaxation times of 10, 20, 30, 40, 50 and 80 ms respectively were 32.75 g/L, 16.083 g/L, 10.563 g/L, 7.588 g/L, 6.242 g/L and 3.847 g/L, and are based on calculations proposed by Schenck.²⁵

Field perturbations with magnitude and spatial distributions similar to those induced by breathing were created during the image acquisition by manually moving a water bottle (5 L) approximately sinusoidally with a period of 5 s between 54 and 65 cm distance from the isocenter along the z direction. A 2D single-slice T_2^* -weighted multigradient echo sequence (10 echoes) with scan parameters $T_R/T_E/\Delta T_E/\text{flip angle} = 400 \text{ ms}/4\text{--}33 \text{ ms}/3 \text{ ms}/20^\circ$, pixel size = $0.5 \times 0.5 \text{ mm}^2$, FOV = $130 \times 130 \text{ mm}^2$, slice thickness = 2 mm, acquisition time = 1 min 45 s was applied. The phantom was imaged in the transverse plane in the middle of the vials after third-order static shimming, which was then held constant for the rest of the session. Phantom scans were repeatedly acquired under three conditions: without field perturbations and without field stabilization, referred to as “reference scan,” and twice with field perturbations, once with and once without field stabilization. The scans were repeated ten times under each of the above described conditions.

2.4 | *In vivo* experiments

The study was approved by the local ethics board. Informed consent was obtained from six healthy subjects (three male, mean age 29 years). For the assessment of real-time field control and its potential benefit to T_2^* mapping *in vivo*, a T_2^* -weighted multigradient echo sequence (10 echoes) with scan parameters $T_R/T_E/\Delta T_E/\text{flip angle} = 600 \text{ ms}/5\text{--}56 \text{ ms}/6 \text{ ms}/20^\circ$, pixel size = $0.7 \times 0.7 \text{ mm}^2$, FOV = $200 \times 200 \text{ mm}^2$, five slices, 2.5 mm

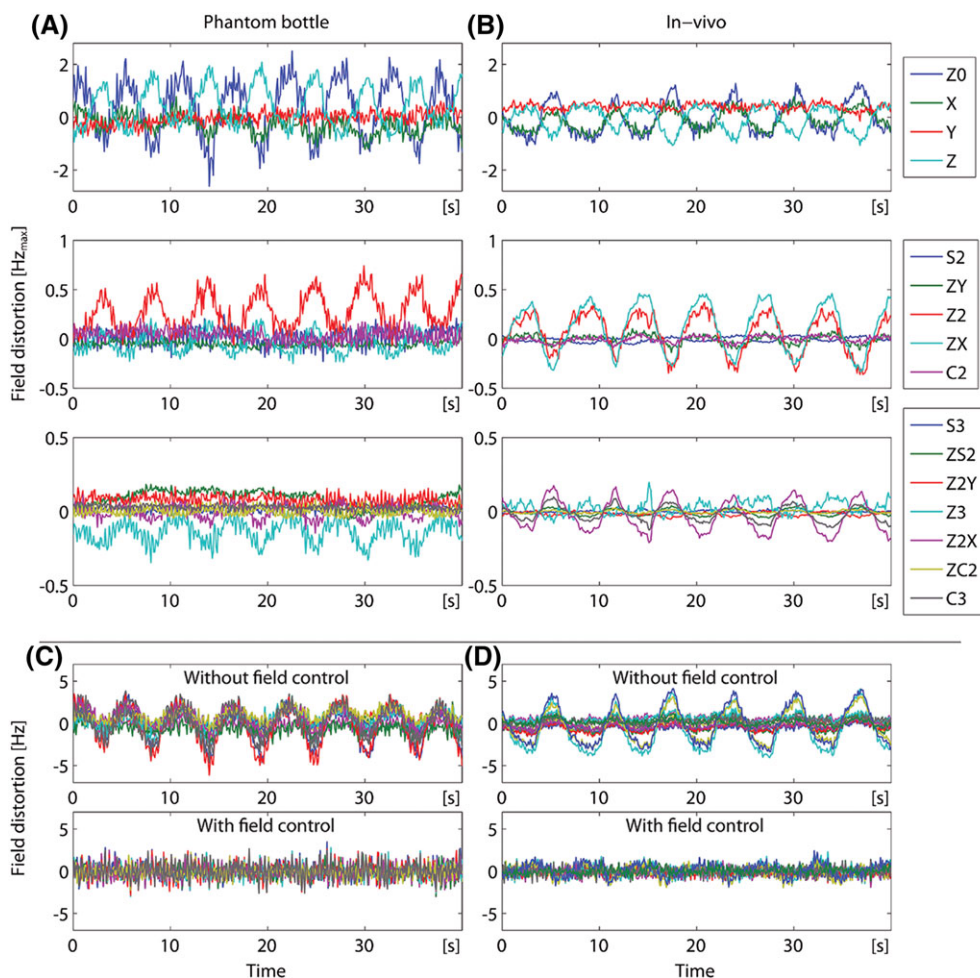


FIGURE 2 A,B, Field dynamics decomposed into the different shim terms (third-order spherical harmonics). X, anterior-posterior; Y, left-right; Z, head-feet. The field dynamics were measured during simulated breathing by moving a water phantom A, and during an *in vivo* experiment B. The plots show the maximum effect relating to each shim term within the imaging volume. C,D, Field changes in all 16 field probes of phantom C, and *in vivo* D, experiments with and without field control

slice thickness, 0.5 mm gap, acquisition time = 2 min 53 s was acquired in all volunteers. After a scout scan, an acquisition plane positioned in the transverse orientation, aligned in parallel to a straight connection between anterior and posterior commissure, was described. The static magnetic field was optimized within a user-defined region covering all slices using a third-order FASTMAP shimming procedure.²⁶ The experiments were repeated a minimum of four times under both conditions (with and without field stabilization) with a per-subject randomly selected condition order.

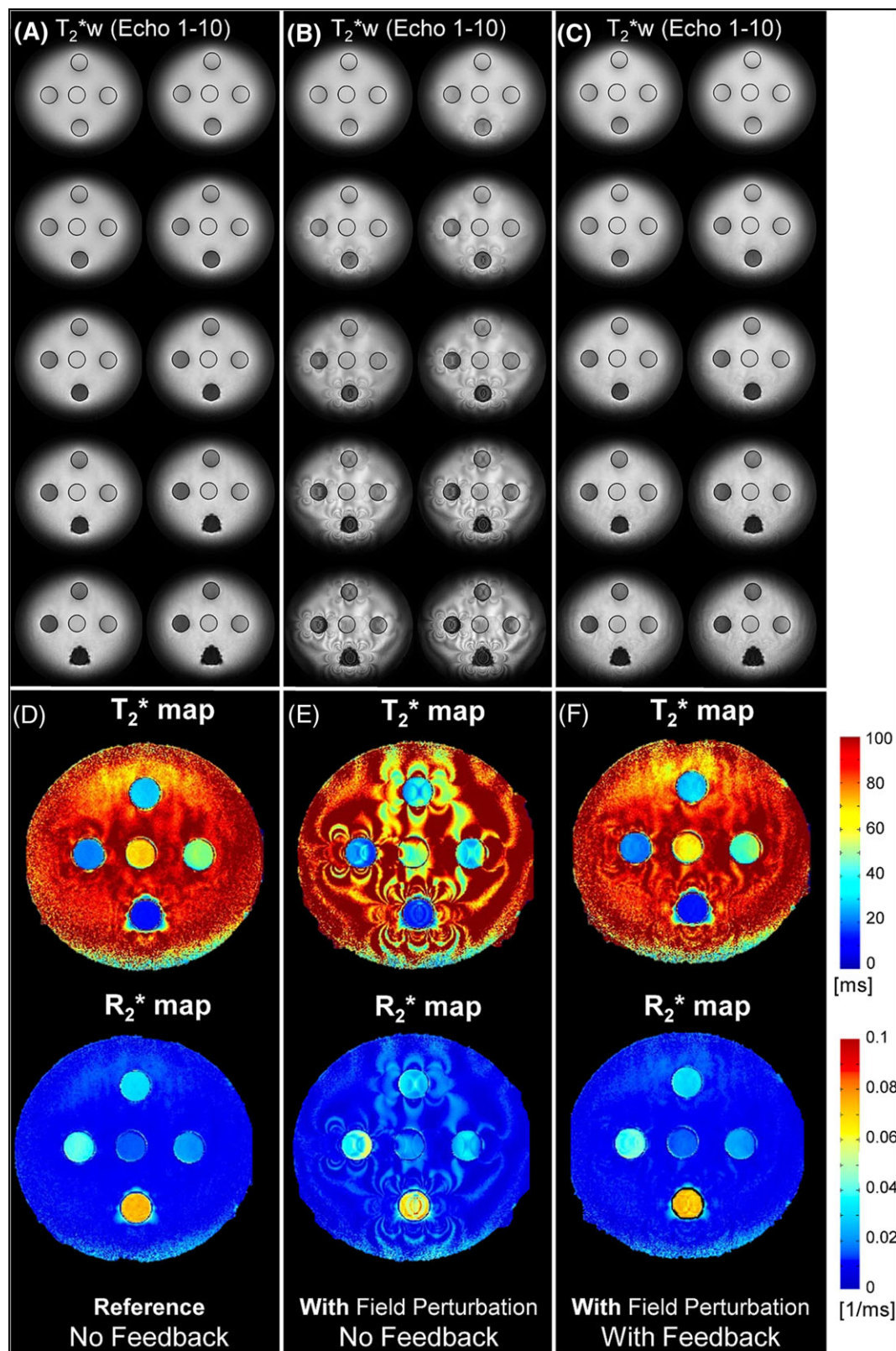


FIGURE 3 T_2^* -weighted images for the 10 acquired echo times A-C, and resulting T_2^* and R_2^* maps D-F. The images were collected in experiments without field perturbations (reference) A,D, with induced field perturbation but without feedback field control B,E, or with induced field perturbation and with feedback control C,F

The distribution was four repetitions (one subject), five repetitions (two subjects) and six repetitions (three subjects). The volunteers were asked to breathe normally during the whole scanning session.

2.5 | R_2^*/T_2^* quantification

2.5.1 | R_2^* fitting

To define the region of interest (ROI) for R_2^* fitting, a threshold was applied to the magnitude images at the first echo. The multi-echo MR signal intensity as a function of the echo time, $S(T_E)$, was fitted pixel-wise to the expression $\ln S(T_E) = \ln S(T_E = 0) - R_2^* \cdot T_E$ using the *polyfit* function of the Python *numpy* package, Version 1.9.2, in a linear least-squares polynomial regression. To reduce the effect of noise on the fitted result, sums of weighted least squares were minimized during the fit, using the original magnitude images as weights. Finally, T_2^* was obtained by inversion: $T_2^* = 1/R_2^*$. As a measure for the fit residuals and the goodness of the fits, normalized root mean squared errors, NRMSE values, were calculated for each voxel, according to

$$\text{NRMSE} = \sqrt{\frac{\left(\sum_{i=1}^{N_{T_E}} (S(T_{E_i}) - S_{\text{fit}}(T_{E_i}))^2 \right)}{(N_{T_E} - 2)}} / S_{\text{fit}}(0)$$

where N_{T_E} is the number of acquired echoes and $S_{\text{fit}}(T_{E_i})$ denotes the fitted signal intensity at echo time T_{E_i} . The division by the estimated signal intensity at zero echo time allowed a better comparison of the fitting errors across image regions with strongly differing initial signal intensity.

2.5.2 | Repeatability

To evaluate the robustness of the determined T_2^* values across several repetitions of the measurements, pixel-wise mean T_2^* values and their standard deviations across the repetitions were calculated for both conditions (with and without field control) using MATLAB® (R12b, MathWorks,

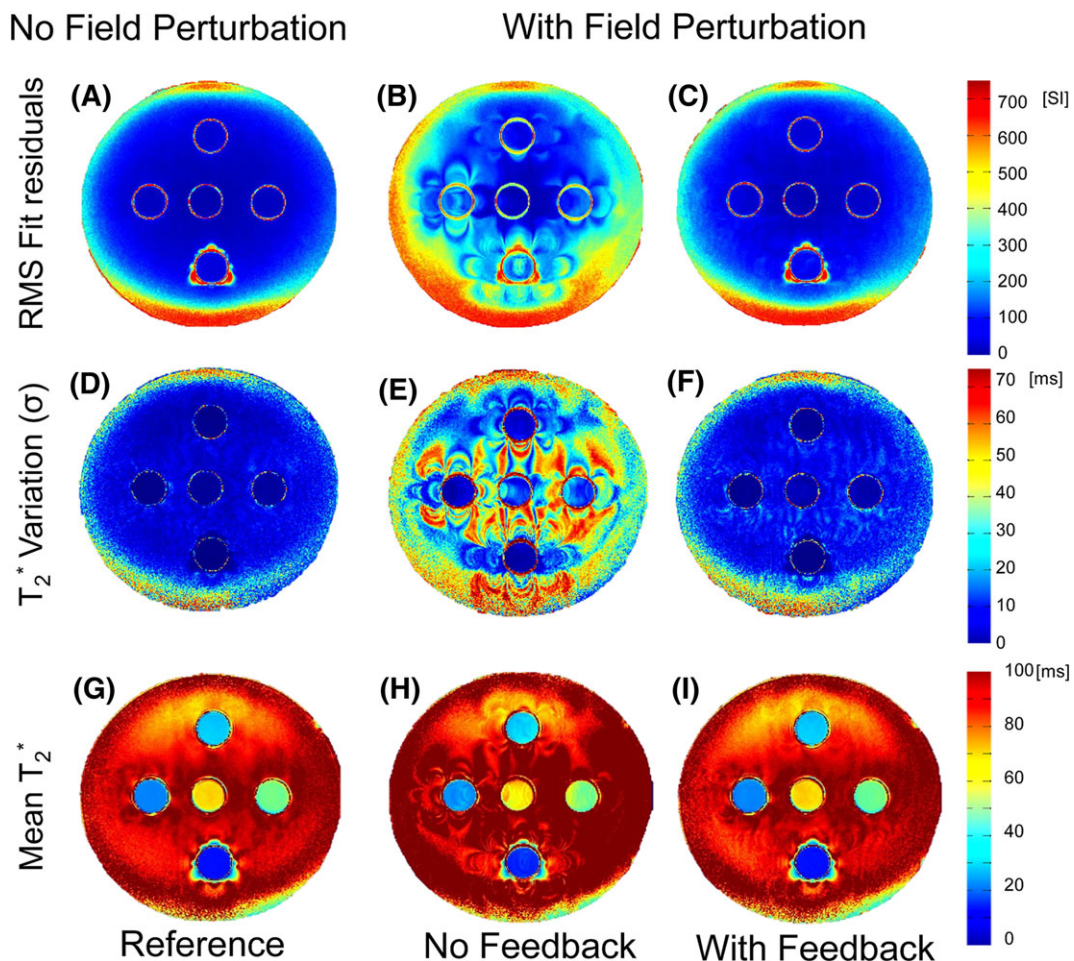


FIGURE 4 Statistical evaluations of the repeated measurements. The data was collected in experiments without field perturbations (reference) A, D, G, with induced field perturbation but without feedback field control B, E, H or with induced field perturbation and with feedback control C, F, I. A-C, The normalized RMS error map of the fit residuals. D-F, The standard deviation over the repeated experiments. G-I, mean T_2^* maps

Natick, MA, USA) after intra-subject realignment (MATLAB routines from the Wellcome Department of Cognitive Neurology, London, <http://fil.ion.ucl.ac.uk/spm>) of all subsequently acquired maps to those of the first series, to account for displacement of anatomy between scan repetitions.

As a measure for the root mean squared fit errors across repetitions, separate pixel-wise RMS_{fit} residuals (RMS_{fr}) maps were calculated for both conditions (with and without field control) according to

$$\text{RMS}_{\text{fr}} = \sqrt{\frac{\left(\sum_{r=1}^{N_r} \text{NRMSE}_r^2\right)}{N_r}}$$

where N_r denotes the total number of repetitions.

For the phantom data an ROI-based analysis was performed: on the first T_2^* maps a circular ROI was drawn on each of the five vials and copied to all T_2^* maps subsequently acquired in repeated measurements, using the vendor-supplied analysis tool on the MRI console. The inter-repetition variation of the mean T_2^* value within each vial or ROI was calculated and visualized by boxplots.

TABLE 1 Average T_2^* variation and RMS of the fit residuals from one (middle) slice

	T_2^* variation (σ) [ms]			RMS T_2^* fit residuals [SI]		
	No feedback	With feedback	Reduction (%)	No feedback	With feedback	Reduction (%)
Phantom	35.57	15.31	57	290.91	176.10	39
Subject 1	4.78	4.10	14	75.96	68.54	10
Subject 2	4.13	4.12	0	60.37	58.12	4
Subject 3	2.23	1.92	14	66.07	63.03	5
Subject 4	4.51	4.21	7	75.53	69.58	8
Subject 5	5.65	4.27	25	84.09	66.67	21
Subject 6	5.46	4.11	25	93.93	81.59	13

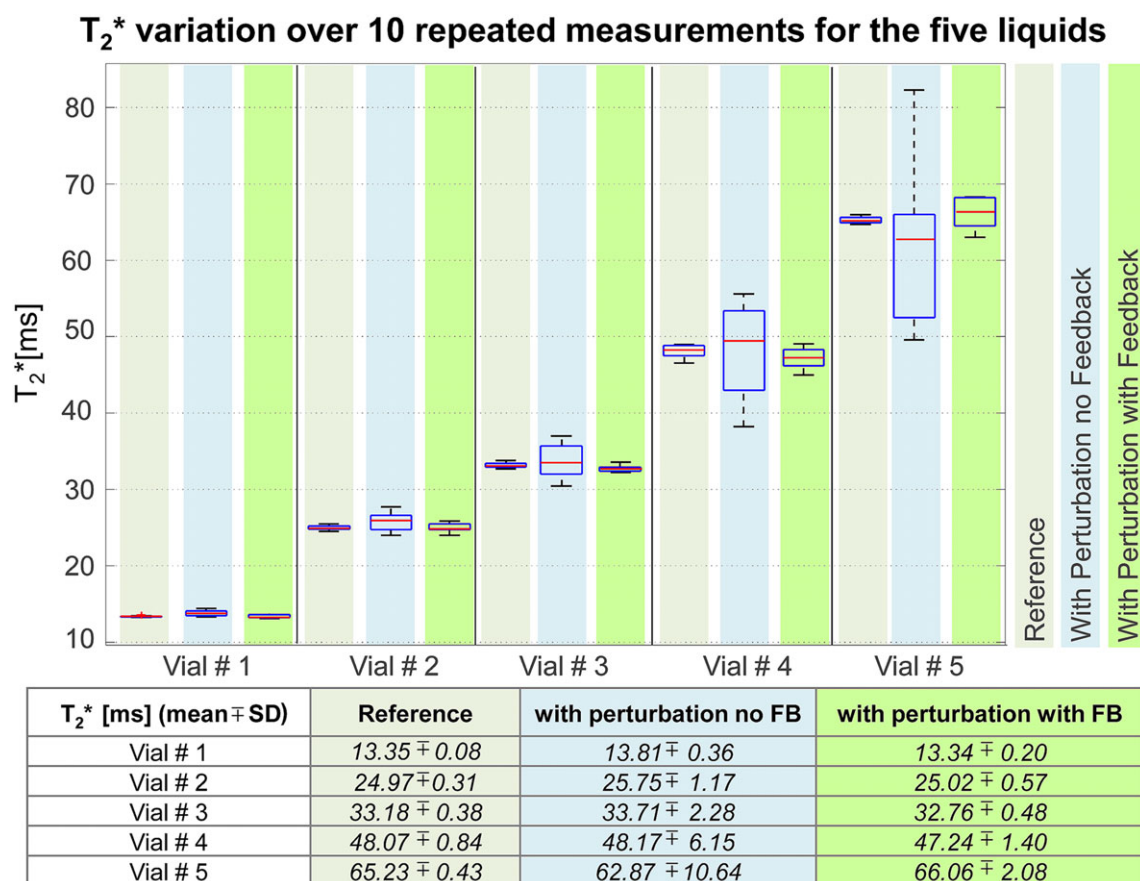


FIGURE 5 Variation of obtained T_2^* values over 10 repeated measurements in the five liquids (Vials 1–5). The data was collected in experiments without field perturbations (reference) (light brown), with induced field perturbation but without feedback field control (light blue) or with induced field perturbation and with feedback control (green). The boxplots indicate the median (red), 25th and 75th percentiles (blue box) and minimum and maximum values (whiskers). Mean T_2^* and standard deviation values for all liquids for all three experiments are indicated in the table below

3 | RESULTS

3.1 | Field distortions and control

Most significant field distortions created by the moving water bottle and from volunteer's respiration were of zeroth (B_0) and first (X and Z) order. Field changes were also in higher (second and third)-order spherical harmonics (Figure 2A,B). Spherical harmonic terms including Z (head-feet) and X (anterior-posterior) directions were stronger than terms depending on Y (left-right). Field changes measured by all 16 probes individually show the pattern of the artificially induced field perturbation with the water bottle and from the subject's respiration (Figure 2C,D). A stabilization of the

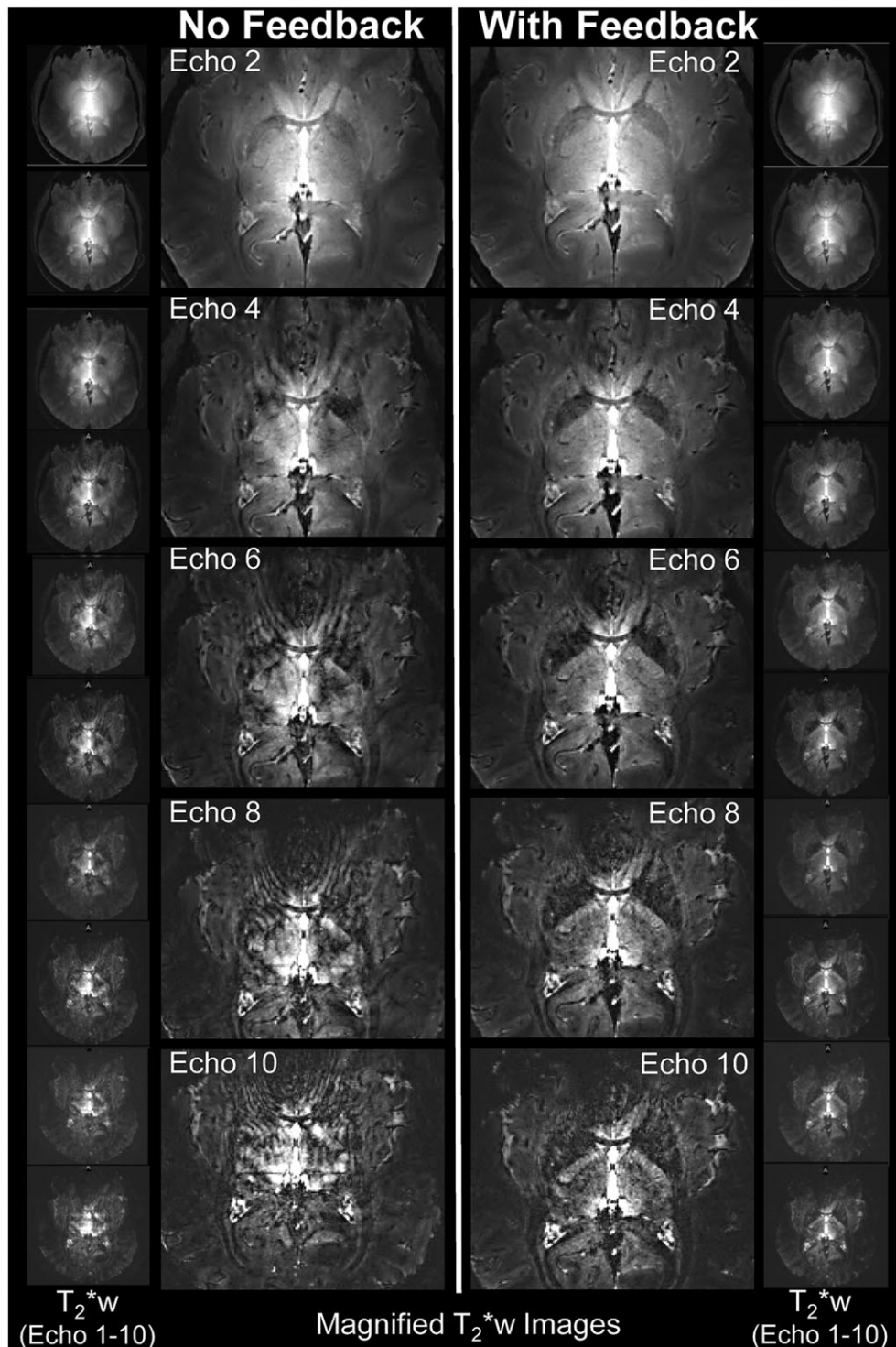


FIGURE 6 *In vivo* T_2^* -weighted images of an exemplary measurement of one subject without (left) and with (right) feedback field control (Echoes 1–10, Slice 3) and magnified versions (central columns, even images only). Ringing artifacts around the nasal cavities and signal intensity variations between corresponding (left/right hemisphere) structures such as the thalamus or within the putamen and globus pallidum are removed by field stabilization

magnetic field during the scan could be achieved with real-time field control in the phantom and the *in vivo* experiments (Figure 2C,D). Field perturbations were similar to those previously reported by Duerst et al.²¹ Maximum field distortions caused by normal breathing were in the range of 4 Hz to 12 Hz (peak to peak) observed in zeroth- and first-order spherical harmonics in this volunteer group. Field changes *in vivo* without field control measured in all 16 probes were comparable to the field perturbations in the phantom experiments in terms of amplitude and frequency (Figure 2D). Field control effectively reduced these field variations and stabilized the field during the scan (Figure 2D). The remaining field fluctuations when using field stabilization are field changes with frequencies above the feedback system closed-loop bandwidth and were therefore not corrected (Figure 2C,D). Field perturbations could be simulated well with the moving water bottle in the phantom experiments. Characteristics and amplitude of the artificially introduced field changes were comparable to the field changes measured *in vivo*. However due to the use of different field probes for the phantom experiments and the *in vivo* experiments, the measurements of the phantom experiments appear more noisy. The reason is the difference in T_1 relaxation of the NRM field probes and the different sampling time of the probe signal.

3.2 | Phantom measurements

Without field control, breathing-type field fluctuations caused by the moving water bottle induced strong ghosting artifacts in the T_2^* -weighted source images (Figure 3B) that were especially prominent at longer echo times (>17 ms) and in the resulting relaxation maps (R_2^* , T_2^*). Field control removed these artifacts almost entirely from the source images (Figure 3C), achieving similar image quality as in the reference experiment (Figure 3A). The improved field stabilization also propagates positively to the resulting T_2^* and R_2^* maps (Figure 3F). The disturbing artifacts in the relaxation maps without field control (Figure 3E) were remarkably reduced by the active field control (Figure 3F), resulting in maps that were comparable to those of the reference experiments (Figure 3D). Figure 4 shows pixel-wise RMS_{fr} (A-C), standard deviations (D-F) and mean T_2^* values (G-I) obtained from the 10-fold repeated measurements. Reference data collected without field perturbation, (Figure 4A,D,G) as well as data acquired under field perturbation without (Figure 4B,E,H) and with active field control (Figure 4C,F,I) are shown. The RMS_{fr} was clearly increased by field perturbation in the absence of active field control. In particular, a large variation of T_2^* times was introduced by field perturbation, which is prominently visualized in the corresponding standard deviation maps. Feedback field control during field perturbation reduced this variation by 57% for the standard deviations and by 39% for the RMS_{fr} values when averaged over a whole brain slice (Table 1). This finding is visually

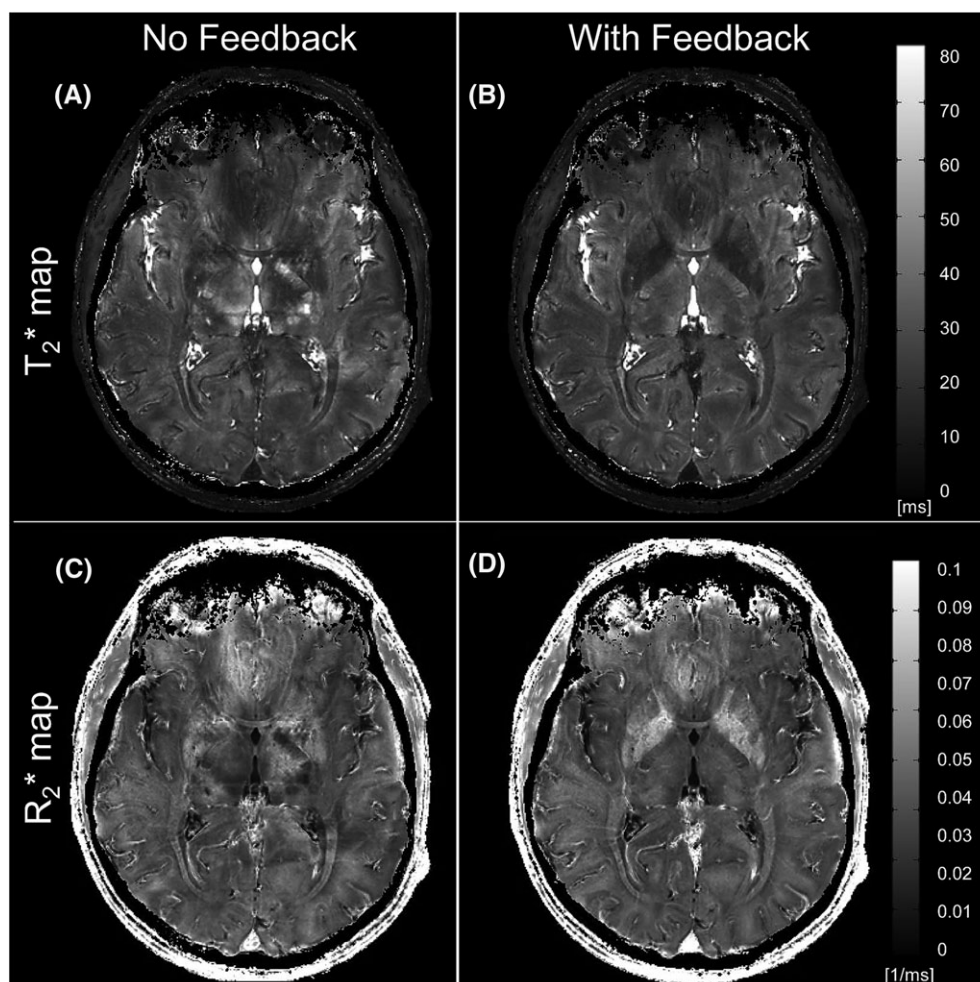


FIGURE 7 T_2^* and R_2^* maps obtained from the T_2^* -weighted images shown in Figure 6 without A,C, and with B,D, feedback field control

confirmed in a comparison of the statistical maps obtained under field perturbation with and without active field control (Figure 4C,F) with those from the reference experiments (Figure 4A,D). An ROI-based analysis of T_2^* across 10 measurement repetitions for all five liquids is plotted in Figure 5. The box plots confirmed a strong decrease in the spread of T_2^* estimates for all relaxation times when field control during field perturbation was switched on. Compared with the data variation during field perturbation without field stabilization, in the middle plot of each group, the precision of the measurement is remarkably improved when applying real-time field stabilization.

3.3 | In vivo measurements

In the source images, different types of artifact such as ringing, signal loss, ghosting and darkening/shading have been observed. Most of these artifacts are described in more detail in the work of Duerst et al.²¹ The severity of most of the artifacts apparent in the source images scaled with the echo time and became particularly prominent at echo times longer than 25 ms (Figure 6, Echoes 6–10).

Under feedback field control, a reduction of the overall artifact level in the source images was observed. Figure 6 demonstrates the impact of field control on source images. Image quality was greatly improved by field control, particularly at longer echo times (Echoes 6–10).

The reduction of the artifact level translates into the resulting quantitative maps (Figure 7). Strong and disturbing ghosting artifacts, ringing artifacts and shading/darkening (thalamus, putamen, globus pallidus) in T_2^* and R_2^* maps shown in one subject were effectively removed from the quantitative maps by field stabilization (Figure 7).

The extension of the apparent signal loss in the vicinity of the paranasal sinuses, as well as ringing (wave-like intensity modulations), were reduced in the T_2^* -weighted source images by field control (Figure 8A–C). Shading/darkening of brain tissue appeared haphazardly in various brain regions and was also diminished by field control (Figure 8D,E).

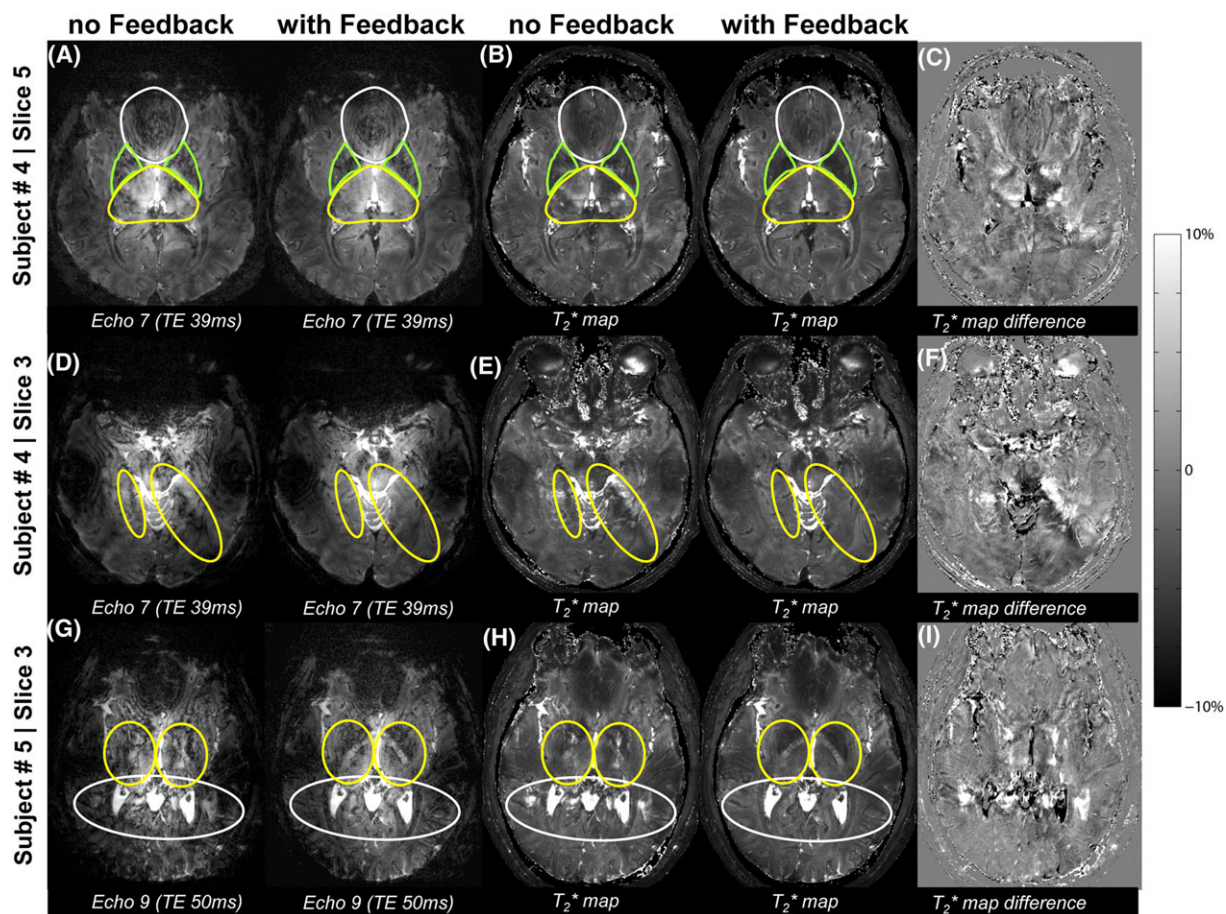


FIGURE 8 Different types of artifact and their appearance on the source images and on corresponding quantitative T_2^* maps with and without feedback. A–C, Intensity modulation “ringing artifact” (white demarcation) on source images A, at echo time 39 ms and on T_2^* maps B, around the paranasal sinuses. These signal modulations are also disturbing the putamen and globus pallidus (green demarcation) in both hemispheres. The extension of the accompanying signal loss around the paranasal sinuses (yellow demarcation) is reduced on the source images as well as on corresponding T_2^* maps with field control A,B. The thalamus (yellow demarcation) suffered from ghosting from CSF (third ventricle) and from signal loss. D–F, Shading/darkening on source images D, and T_2^* maps E, of the same subject (as in A–C), but on a different slice level. G–I, Ghosting artifact from CSF in the third ventricle (yellow circles) and fourth ventricle (white circle). Difference images (with and without feedback) C,F,I, show the reduction of artifacts in the T_2^* maps when using field control. Difference images are scaled to the maximum of the corrected image

The CSF of the ventricles was a main source of ghosting artifacts. Field control reduced ghosting in the source images. This was most apparent in structures such as the thalamus or globus pallidus (Figure 8A-C, G-I) and other brain regions around the ventricles (Figure 8G-I). Ghosting artifacts were introduced at very long echo times of more than 40 ms (Figure 6, Figure 8G). T_2^* maps of individual scans from three subjects show the improvement of image quality obtained with field stabilization using feedback field control (Figure 9).

For the assessment of standard deviation and fitting precision just one slice (midslice) was evaluated for each volunteer, since the lower and upper slices were in part corrupted after co-registration in SPM. A substantially reduced T_2^* variation across the 10 measurement repetitions was observed (Figure 10). On average, active field control achieved a reduction of 15% ($p = 0.036$) of the mean standard deviation in a whole brain slice over all subjects (Table 1). The RMS_{fr} was on average 10% smaller ($p = 0.019$) with field control (Table 1). RMS_{fr} maps from three different subjects show the reduction of fitting errors when using field control (Figure 11).

4 | DISCUSSION

In this work the negative impact of field perturbations on T_2^* quantification in the human brain at 7 T was investigated and the potential of an active real-time higher-order field control system for mitigation of this impact was explored. In agreement with the previous report,²¹ the artifact severity

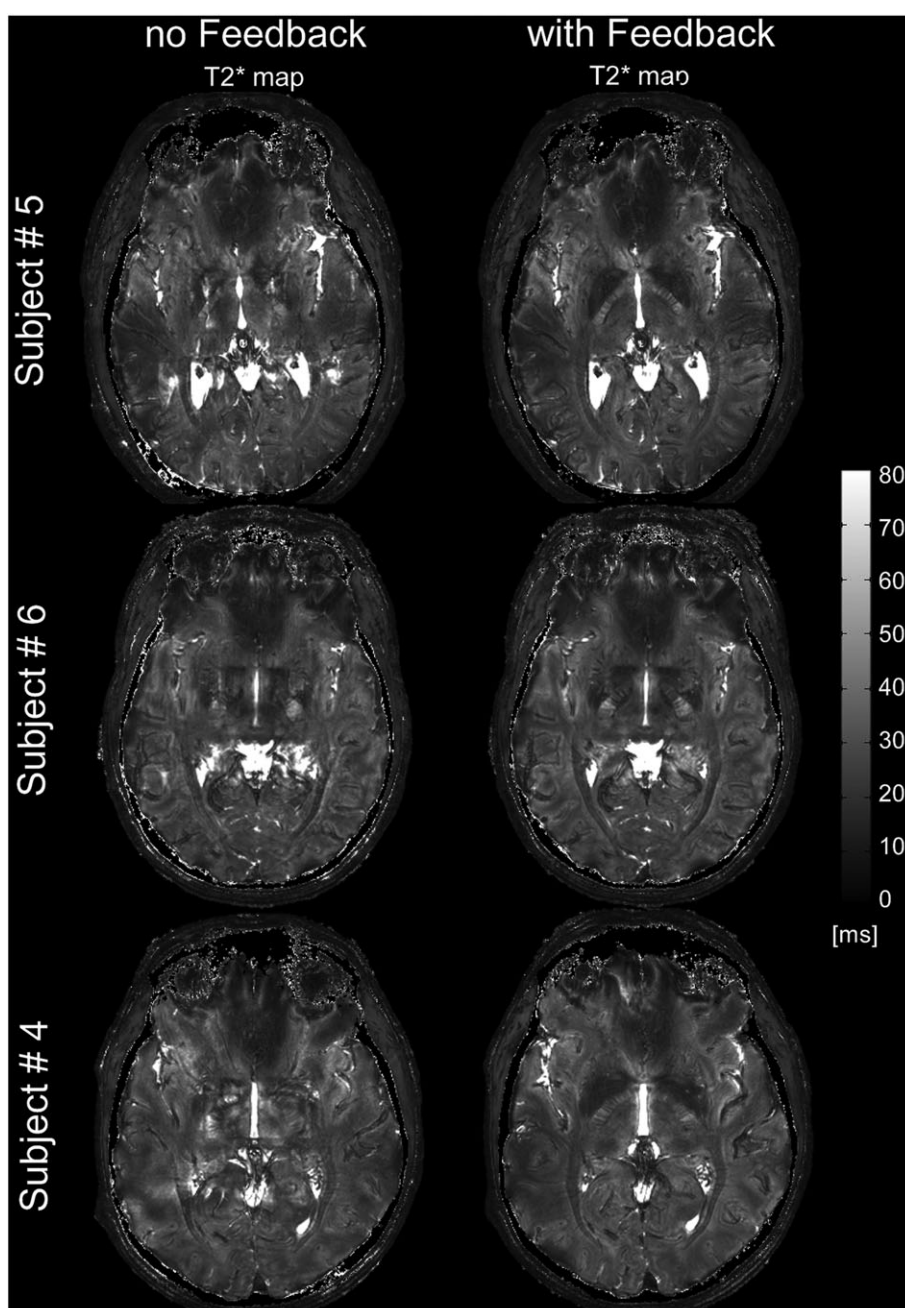


FIGURE 9 T_2^* maps from a single measurement (midslice) without and with feedback field control for three subjects

in the source images was found to depend on the examined subject's physical constitution, cooperation and breathing pattern. Furthermore, the severity of most artifacts scaled with the echo time due to the accumulation of phase errors.

Artifacts in the source images were found to propagate to the quantitative relaxation-parameter (T_2^*/R_2^*) maps in different ways. Some, e.g. signal loss, shading or darkening, and ghosting that appeared in one or a few source images, were directly and equivalently seen in the quantitative maps. Others, such as ringing or intensity modulations that appeared on all or most source images, were reflected in a different, typically more diffuse and indirect, way in the quantitative maps. This is most probably due to an averaging effect inherent in the T_2^* fitting across signal intensities in images acquired at all echo times.

Many brain structures, e.g. caudate nucleus, thalamus, globus pallidus or putamen, are located in the close vicinity of regions with strong magnetic field gradients caused by susceptibility differences, e.g. between air in frontal cavities and brain tissue or between tissue and petrosal bone. In combination with spatiotemporal field changes, e.g. caused by subject breathing, an increase of ringing artifacts around the affected anatomical regions was observed. These ringing artifacts in the source images translate into the corresponding quantitative maps as local fuzziness/blurriness, leading to corrupted or poorly defined tissue borders. The reduction of spatiotemporal field changes decreases the signal modulation in the source images and improves tissue border definition/image sharpness in the final quantitative relaxation maps. Ghosting of structures with high signal intensity (e.g. CSF) in the phase encoding direction are probably caused by more global (far-range) temporal magnetic field variations. This artifact

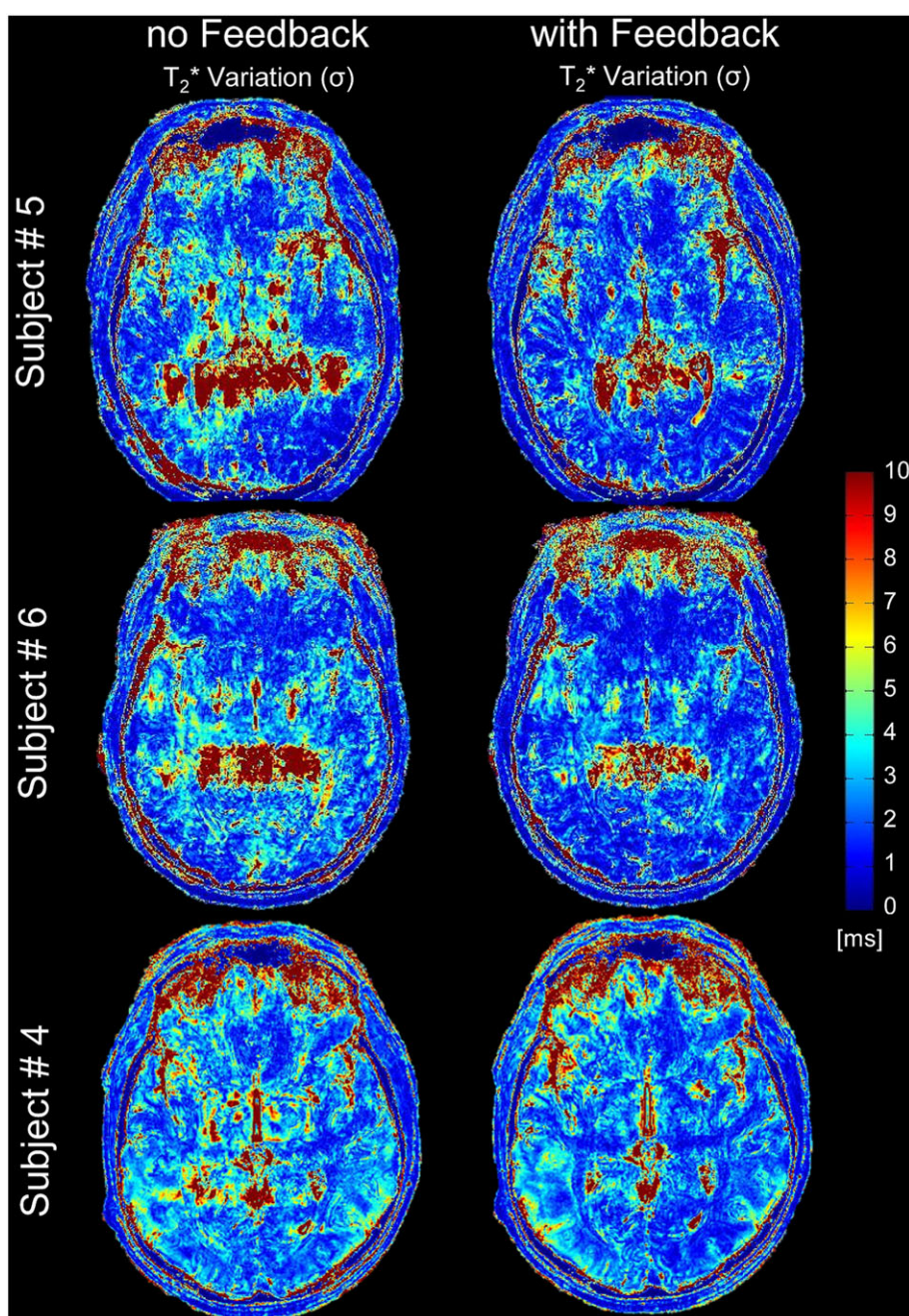


FIGURE 10 T_2^* variation (standard deviation) across all repeated measurements without and with feedback field control for three subjects

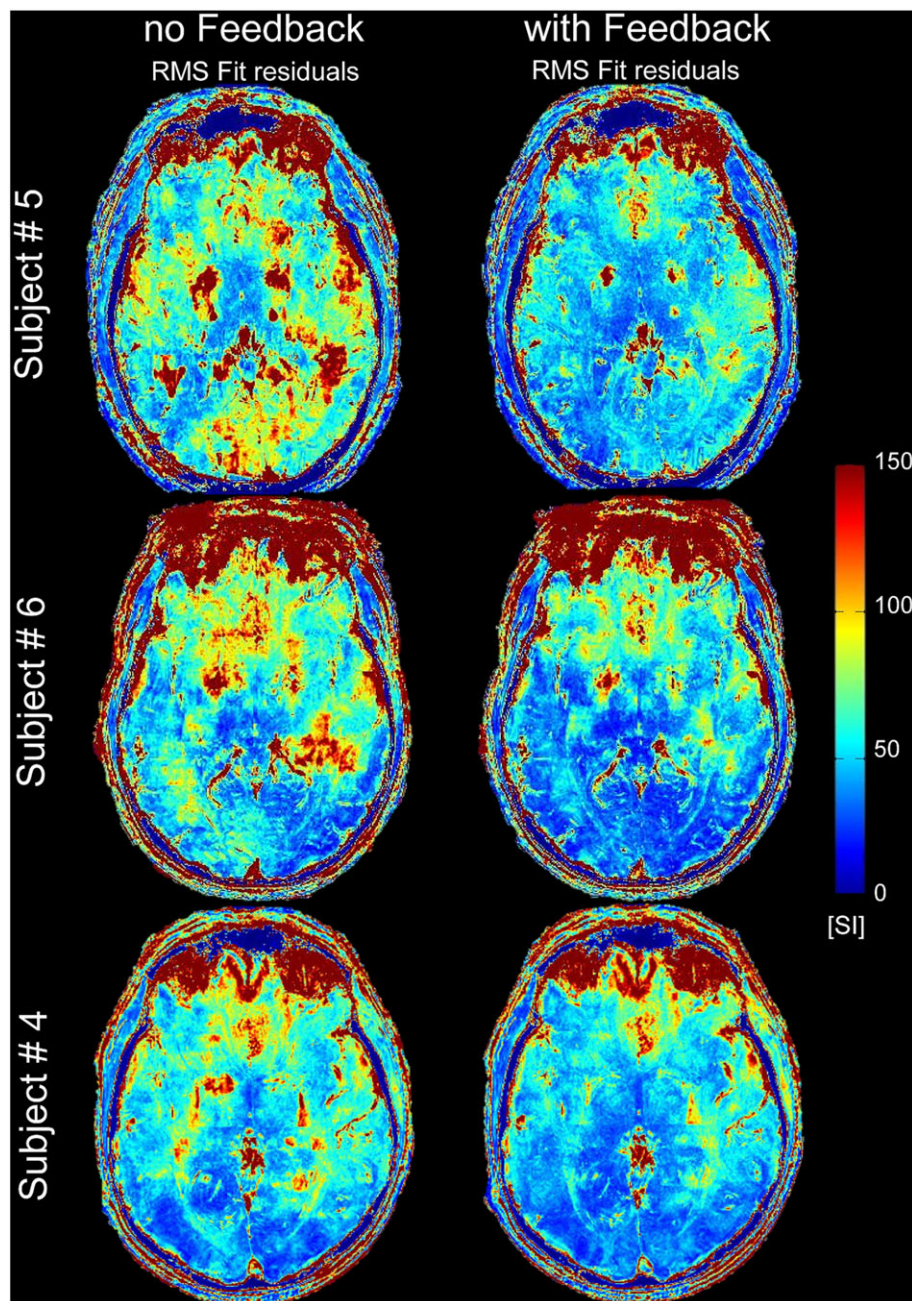


FIGURE 11 Normalized RMS of the fit residuals over all repeated measurements without and with feedback field control for three subjects

is emphasized if tissue with a long T_2^* relaxation time is neighbor to—in the phase encoding direction—tissue with a short T_2^* relaxation time. Depending on the frequency of occurrence in the source images and on the surrounding tissue signal intensity, ghosting in the final maps appears differently: clearly recognizable as ghosting (artifact present on few source images only) or as fuzziness/blurriness (intermediate or high signal intensity of surrounding tissue, or artifact present on many source images).

The precision of T_2^* mapping increases with field stabilization since it allows the acquisition of better source images at longer echo times by minimizing the accumulation of phase errors. Feedback field control extenuates fitting errors through field stabilization, which translates into more robust, reliable and accurate T_2^* quantification. It is noteworthy that the improvement of T_2^* quantification achieved by feedback field stabilization showed a substantial inter-subject variation: whereas in one subject no reduction of the observed T_2^* standard deviation and only a minor reduction of 4% RMS_{fr} was found, the corresponding values were highly significant in another subject, where feedback field control achieved reductions of $\sim 25\%$ SD and $\sim 21\%$ RMS_{fr} .

The technique also has potential in clinical studies, where certain patient populations have been shown to induce particularly challenging field changes related to their breathing pattern.⁸ The influence of exterior field contributions, e.g. due to nearby railway lines, was not examined in this work, but similar benefits may be expected from the proposed technique.

ACKNOWLEDGEMENT

The authors are grateful for financial support of this work by the Swiss Commission for Technology and Innovation.

REFERENCES

1. Haacke EM, Cheng NYC, House MJ, et al. Imaging iron stores in the brain using magnetic resonance imaging. *Magn Reson Imaging*. 2005;23(1):1-25. <https://doi.org/10.1016/j.mri.2004.10.001>
2. Peters AM, Brookes MJ, Hoogenraad FG, et al. T_2^* measurements in human brain at 1.5, 3 and 7 T. *Magn Reson Imaging*. 2007;25(6):748-753. <https://doi.org/10.1016/j.mri.2007.02.014>
3. Ordidge RJ, Gorell JM, Deniau JC, Knight RA, Helpert JA. Assessment of relative brain iron concentrations using T_2 -weighted and T_2^* -weighted MRI at 3 Tesla. *Magn Reson Med*. 1994;32(3):335-341. <https://doi.org/10.1002/mrm.1910320309>
4. Gelman N, Gorell JM, Barker PB, et al. MR imaging of human brain at 3.0 T: preliminary report on transverse relaxation rates and relation to estimated iron content. *Radiology*. 1999;210(3):759-767. <https://doi.org/10.1148/radiology.210.3.r99fe41759>
5. Schenck JF, Zimmerman EA. High-field magnetic resonance imaging of brain iron: birth of a biomarker? *NMR Biomed*. 2004;17(7):433-445. <https://doi.org/10.1002/nbm.922>
6. Govindarajan ST, Cohen-Adad J, Sormani MP, Fan AP, Louapre C, Mainero C. Reproducibility of T_2^* mapping in the human cerebral cortex in vivo at 7 tesla MRI. *J Magn Reson Imaging*. 2015;42(2):290-296. <https://doi.org/10.1002/jmri.24789>
7. Cohen-Adad J. What can we learn from T_2^* maps of the cortex? *Neuroimage*. 2014;93(Part 2):189-200. <https://doi.org/10.1016/j.neuroimage.2013.01.023>
8. Versluis MJ, Peeters JM, van Rooden S, et al. Origin and reduction of motion and f_0 artifacts in high resolution T_2^* -weighted magnetic resonance imaging: application in Alzheimer's disease patients. *Neuroimage*. 2010;51(3):1082-1088. <https://doi.org/10.1016/j.neuroimage.2010.03.048>
9. van Gelderen P, de Zwart JA, Starewicz P, Hinks RS, Duyn JH. Real-time shimming to compensate for respiration-induced B_0 fluctuations. *Magn Reson Med*. 2007;57(2):362-368. <https://doi.org/10.1002/mrm.21136>
10. Van de Moortele P-F, Pfeuffer J, Glover GH, Ugurbil K, Hu X. Respiration-induced B_0 fluctuations and their spatial distribution in the human brain at 7 Tesla. *Magn Reson Med*. 2002;47(5):888-895. <https://doi.org/10.1002/mrm.10145>
11. Raj D, Anderson AW, Gore JC. Respiratory effects in human functional magnetic resonance imaging due to bulk susceptibility changes. *Phys Med Biol*. 2001;46(12):3331. <https://doi.org/10.1088/0031-9155/46/12/318>
12. Birn RM, Bandettini PA, Cox RW, Jesmanowicz A, Shaker R. Magnetic field changes in the human brain due to swallowing or speaking. *Magn Reson Med*. 1998;40(1):55-60. <https://doi.org/10.1002/mrm.1910400108>
13. Barry RL, Williams JM, Klassen LM, Gallivan JP, Culham JC, Menon RS. Evaluation of preprocessing steps to compensate for magnetic field distortions due to body movements in BOLD fMRI. *Magn Reson Imaging*. 2010;28(2):235-244. <https://doi.org/10.1016/j.mri.2009.07.005>
14. Versluis MJ, Sutton BP, de Bruin PW, Börner P, Webb AG, van Osch MJ. Retrospective image correction in the presence of nonlinear temporal magnetic field changes using multichannel navigator echoes. *Magn Reson Med*. 2012;68(6):1836-1845. <https://doi.org/10.1002/mrm.24202>
15. Hu X, Kim SG. Reduction of signal fluctuation in functional MRI using navigator echoes. *Magn Reson Med*. 1994;31(5):495-503.
16. Barmet C, Zanche ND, Pruessmann KP. Spatiotemporal magnetic field monitoring for MR. *Magn Reson Med*. 2008;60(1):187-197. <https://doi.org/10.1002/mrm.21603>
17. Wilm BJ, Barmet C, Pavan M, Pruessmann KP. Higher order reconstruction for MRI in the presence of spatiotemporal field perturbations. *Magn Reson Med*. 2011;65(6):1690-1701. <https://doi.org/10.1002/mrm.22767>
18. Vannesjo SJ, Wilm BJ, Duerst Y, et al. Retrospective correction of physiological field fluctuations in high-field brain MRI using concurrent field monitoring. *Magn Reson Med*. 2015;73(5):1833-1843. <https://doi.org/10.1002/mrm.25303>
19. Duerst Y, Wilm BJ, Dietrich BE, et al. Real-time feedback for spatiotemporal field stabilization in MR systems. *Magn Reson Med*. 2015;73(2):884-893. <https://doi.org/10.1002/mrm.25167>
20. Wilm BJ, Duerst Y, Dietrich BE, et al. Feedback field control improves linewidths in in vivo magnetic resonance spectroscopy. *Magn Reson Med*. 2014;71(5):1657-1662. <https://doi.org/10.1002/mrm.24836>
21. Duerst Y, Wilm BJ, Wyss M, et al. Utility of real-time field control in T_2^* -weighted head MRI at 7T. *Magn Reson Med*. 2015;76(2):430-439. <https://doi.org/10.1002/mrm.25838>
22. De Zanche N, Barmet C, Nordmeyer-Massner JA, Pruessmann KP. NMR probes for measuring magnetic fields and field dynamics in MR systems. *Magn Reson Med*. 2008;60(1):176-186. <https://doi.org/10.1002/mrm.21624>
23. Barmet C, De Zanche N, Wilm BJ, Pruessmann KP. A transmit/receive system for magnetic field monitoring of in vivo MRI. *Magn Reson Med*. 2009;62(1):269-276. <https://doi.org/10.1002/mrm.21996>
24. Dietrich BE, Brunner DO, Wilm BJ, et al. A field camera for MR sequence monitoring and system analysis. *Magn Reson Med*. 2015;75(4):1831-1840. <https://doi.org/10.1002/mrm.25770>
25. Schenck JF. The role of magnetic susceptibility in magnetic resonance imaging: MRI magnetic compatibility of the first and second kinds. *Med Phys*. 1996;23(6):815-850.
26. Gruetter R. Automatic, localized in vivo adjustment of all first- and second-order shim coils. *Magn Reson Med*. 1993;29(6):804-811.

How to cite this article: Wyss M, Duerst Y, Nanz D, et al. Feedback field control improves the precision of T_2^* quantification at 7 T. *NMR in Biomedicine*. 2017;30:e3753. <https://doi.org/10.1002/nbm.3753>